A comprehensive characterization of the time resolution of the Philips Digital Photon Counter

Brunner, S. E.; Gruber, L.; Hirtl, A.; Suzuki, K.; Marton, J.; Schaart, D. R.

DOI
10.1088/1748-0221/11/11/P11004

Publication date
2016

Document Version
Final published version

Published in
Journal of Instrumentation

A comprehensive characterization of the time resolution of the Philips Digital Photon Counter

Published by IOP Publishing for Sissa Medialab

Received: *July 20, 2016*
Revised: *October 1, 2016*
Accepted: *October 25, 2016*
Published: *November 8, 2016*

A comprehensive characterization of the time resolution of the Philips Digital Photon Counter

S.E. Brunner,[a,b,1] **L. Gruber,**[b] **A. Hirtl,**[c] **K. Suzuki,**[b] **J. Marton**[b] **and D.R. Schaart**[a]

[a] *Department of Radiation, Science & Technology, TU Delft, Delft, The Netherlands*
[b] *Stefan Meyer Institute for Subatomic Physics, Austrian Academy of Sciences, Vienna, Austria*
[c] *Institute of Atomic and Subatomic Physics, TU Wien, Vienna, Austria*

E-mail: s.e.k.brunner@tudelft.nl

Abstract: Photodetectors with excellent time resolution are becoming increasingly important in many applications in medicine, high energy- and nuclear physics applications, biology, and material science. Silicon photomultipliers (SiPM) are a novel class of solid-state photodetectors with good timing properties. While the time resolution of analog SiPMs has been analyzed by many groups, the time resolution of the digital photon counter (DPC) developed by Philips has not yet been fully characterised. Here, the timing capabilities of the DPC are studied using a femtosecond laser. The time resolution is determined for complete dies, single pixels, and individual single photon avalanche diodes (SPADs). The measurements cover a broad dynamic range, from intense illumination down to the single-photon level, and were performed at various temperatures between 0°C and 20°C. The measured single photon time resolution (SPTR) ranges from 101 ps FWHM for the DPC3200 sensor pixel to 247 ps FWHM for the DPC6400 sensor die. An extensive study of the single-SPAD time resolution, ranging from single photon to very high laser intensities (~1000 photons per pulse), yielded a time resolution of 48 ps FWHM at the single-photon level.

Keywords: Photon detectors for UV, visible and IR photons (solid-state) (PIN diodes, APDs, Si-PMTs, G-APDs, CCDs, EBCCDs, EMCCDs etc); Gamma camera, SPECT, PET PET/CT, coronary CT angiography (CTA); Instrumentation and methods for time-of-flight (TOF) spectroscopy

[1] Corresponding author.

doi:10.1088/1748-0221/11/11/P11004

Contents

2016 JINST 11 P11004

1 Introduction

In time-of-flight positron emission tomography (TOF-PET), a coincidence resolving time (CRT) at the level of 100 ps would allow a drastic increase of the signal-to-noise ratio in the reconstructed images, whereas ultimate CRTs of 10 ps would enable direct position estimation of the electron-positron annihilation, fundamentally changing the image acquisition methodology. A promising photosensor for improving the time resolution of PET scintillation detectors is the silicon photomultiplier (SiPM) [1]. Besides PET, SiPMs are also expected to find application in high-energy and nuclear physics, biology, and material science (e.g., positron annihilation spectroscopy, PALS).

Using SiPMs in laboratory PET experiments, CRTs below 100 ps FWHM have been reached by several groups [2–5], whereas CRTs in complete whole-body SiPM-based PET scanners are approaching 300 ps FWHM [6, 7]. Considering current detector developments, it is feasible that TOF-PET systems will approach the 100 ps barrier in upcoming years [8–10].

A relatively recent development in solid-state photosensors is the invention of the digital photon counter (DPC) by Philips Digital Photon Counting [11]. Advantages of the DPC concept, such as excellent time resolution, digital addressing of individual SPADs, and on-chip implementation of digital data acquisition and readout electronics, predominate disadvantages arising from the complementary metal-oxide-semiconductor (CMOS) production process used to fabricate the device (e.g., high dark-count rate).

While the time resolution of analog SiPMs has been measured by many groups, the time resolution of the DPC has not yet been fully characterised. Here, we experimentally study the time resolution of the DPC for a wide dynamic range, from the single-photon level up to intense illumination (~1000 photons), and from individual SPADs up to the full die level (see figure 1).

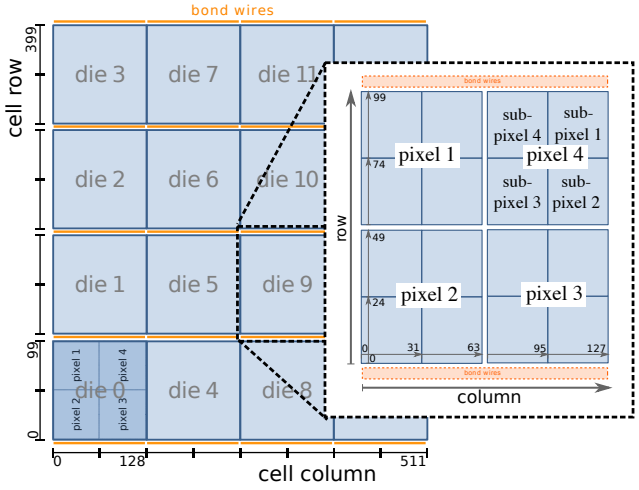

Figure 1. Layout schematics and naming convention of the Philips DPC [12]. The complete sensor tile (left) has an area of 32 mm × 32 mm and is subdivided into 16 dies with an area of 7.9 mm × 7.2 mm each, representing the smallest independent unit of the detector (magnification). Each die is subdivided into 4 pixels with an area of 3.9 mm × 3.2 mm, which again are subdivided into 4 sub-pixels.

2 Method

2.1 The Philips DPC

The Philips DPC is a digital silicon photomultiplier with an active area of 32 mm × 32 mm. It comprises 16 (4 × 4) individual sensor chips called *dies*, see figure 1. Each die contains two time-to-digital converters (TDCs), providing a combined timestamp, and is subdivided into 4 *pixels*, each of them equipped with an individual photon counter. Additionally, the pixels are subdivided into 4 *sub-pixels*, which are connected to the TDCs via a logic network that can be configured to operate with various statistical trigger levels. Rows of SPADs on the sub-pixels are grouped and connected to a programmable validation logic network providing a second, programmable, statistical threshold to validate registered triggers based on the number of fired rows [13].

Two different versions of the DPC-array exist, based on the DPC3200 and DPC6400 sensor dies, respectively. These die types only differ in the size and, therefore, the number of SPADs, i.e., 3200 and 6396 individual SPADs per pixel, respectively. The geometrical layout of the pixels, dies, and the whole detector array remain the same for both array types. An interesting feature of the DPC is the possibility to address and activate or deactivate individual SPADs. This allows to significantly reduce the dark-count rate of the sensor by turning off a small percentage of SPADs with the highest dark-count rates [12]. This option also allows to determine the time resolution of a single SPAD within the sensor.

2.2 Experimental setup & method

A pulsed laser was used for the measurements of the DPC time resolution. The laser was directed onto two dies of the same array (see figure 2). The time resolution was determined by measuring the standard deviation of the time differences between correlated timestamps coming from the two dies. Several configurations were tested in order to obtain a full picture of the DPC time resolution:

2016 JINST 11 P11004

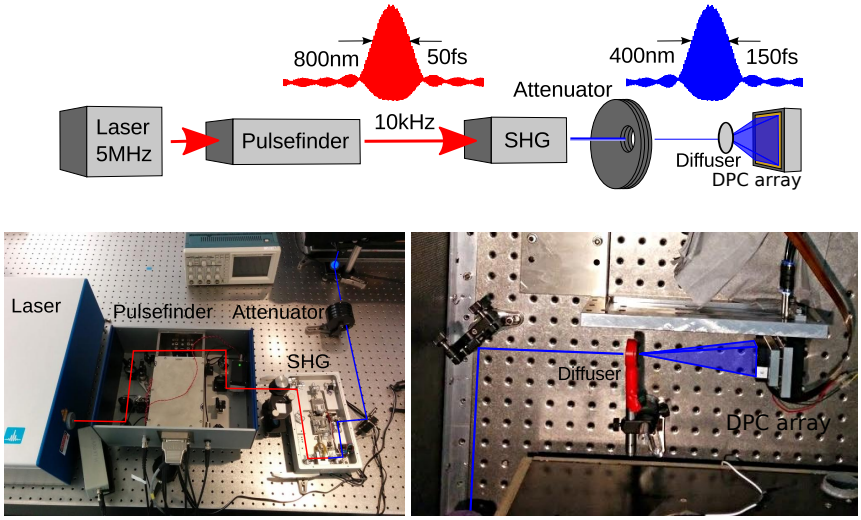

Figure 2. Schematic drawing and pictures of the experimental setup. The laser beam is led through a pulsefinder to adjust the rate to 10 kHz before its wavelength is halved by second harmonic generation (SHG). An attenuator wheel equipped with neutral density filters was used to adjust the laser intensity and a diffuser distributed the beam over the whole area of the DPC array.

- two adjacent dies activated,
- two adjacent pixels (on two adjacent dies) activated,
- two SPADs (on two adjacent dies) activated.

As the time resolution is dependent on the number of detected photons [14, 15], various neutral density filters were used to adjust the laser intensity. To determine the number of photons for each event, the recorded photon counts of the individual pixels were used.

The DPC trigger scheme was set to 1 in all measurements, as this is the only scheme where the absolute value of the trigger threshold is known [13]. For measurements at low laser intensities, i.e., in the range between 0 and 20 photons per laser pulse, the validation logic was deactivated, which means that all events were recorded. At higher laser intensities above 20 photons per pulse the validation was activated to suppress dark-count events and was set to 2. At very high laser intensities (more than 100 photons per pulse), the validation was set to 4. While changing the validation setting did not show any impact on the measured time resolution, it reduced the amount of data recorded per experiment. The coincidence time window was usually set to 4 ns. Furthermore, $2{\times}10^6$ frames were recorded for each setting, where a frame has a duration of 2^{16} clock cycles of 5 ns each. A scheme and pictures of the measurement setup are shown in figure 2.

A fast laser, i. e., a Femtosource XL^{TM} from Femtolasers GmbH, was used for the measurements. This laser provides a power of 650 nJ and a pulse width of 50 fs at 5 MHz repetition rate, with a mean emission wavelength around 800 nm. The emission spectrum of the laser is plotted in figure 3. As the repetition rate of 5 MHz is exceeding the maximum acquisition rate of the DPC, it was reduced to 10 kHz using a Pulsefinder^{TM} from Femtolasers GmbH. After this stage, the laser wavelength was decreased to 400 nm by second harmonic generation (SHG) using a barium borate crystal (BBO). After SHG, the beam traversed a manual optical attenuator wheel equipped with a set

2016 JINST 11 P11004

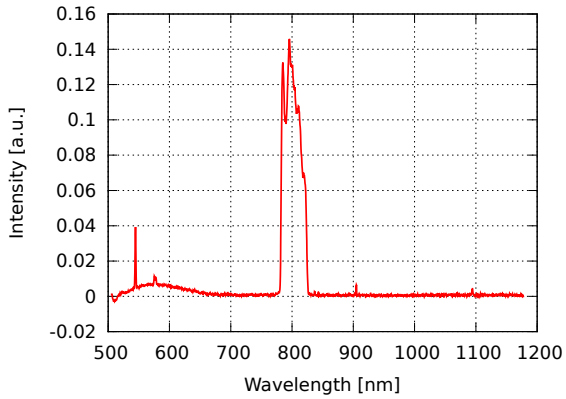

Figure 3. Emission spectrum of the Femtosource XL laser used in the experiments. Data provided by Femtolasers GmbH.

of neutral density filters for precise adjustment of the laser intensity, before it entered a temperature-controlled dark box. After passing an optical diffuser to increase the spatial width, the beam was directed onto the DPC array under test. Due to a compression stage inside the SHG-module, the pulse width after the SHG was approximately 50 fs. With a temporal diffusion of about 20 fs/m and a path length from the SHG to the DPC of 2 – 3 m, a pulse width of approximately 100-150 fs could be expected at the location of the DPC. This value can be considered negligible in comparison to the time resolutions to be measured in this work.

In the following, the time resolution of the DPC was first measured as the standard deviation of a Gaussian fit of the time differences between coincident time-stamps, triggered by the same laser pulse. In general, a coincidence time window of 4 ns was used to select coincident events. Assuming a symmetric setup and Gaussian statistics, the time resolution of a single sensor was determined by dividing by $\sqrt{2}$. Eventually, the single-sensor time resolution is expressed in terms of FWHM by multiplying the single-sensor standard deviation by a factor of 2.35.

3 Results and discussion

3.1 DPC die- and pixel time resolution

Time resolutions were measured for various temperatures and numbers of deactivated cells on die- and pixel-level. Figure 4 shows two plots of the FWHM values obtained for two configurations. The upper half of this figure shows the time resolution of the DPC3200-die at 10°C. The bottom half shows the results for the DPC6400-die at 0°C. For both measurements, the 20 % of cells with the highest dark-count rates were deactivated. The left plots in this figure show the complete data over a broad dynamic range, whereas the plots on the right-hand side show a zoom of the results obtained at low photon counts.

Brunner [16] showed that the time resolution (TR), as a function of the number of photons n, can be described as

$$TR(n) = \frac{p_0}{n^{p_1}} + p_2, \tag{3.1}$$

2016 JINST 11 P11004

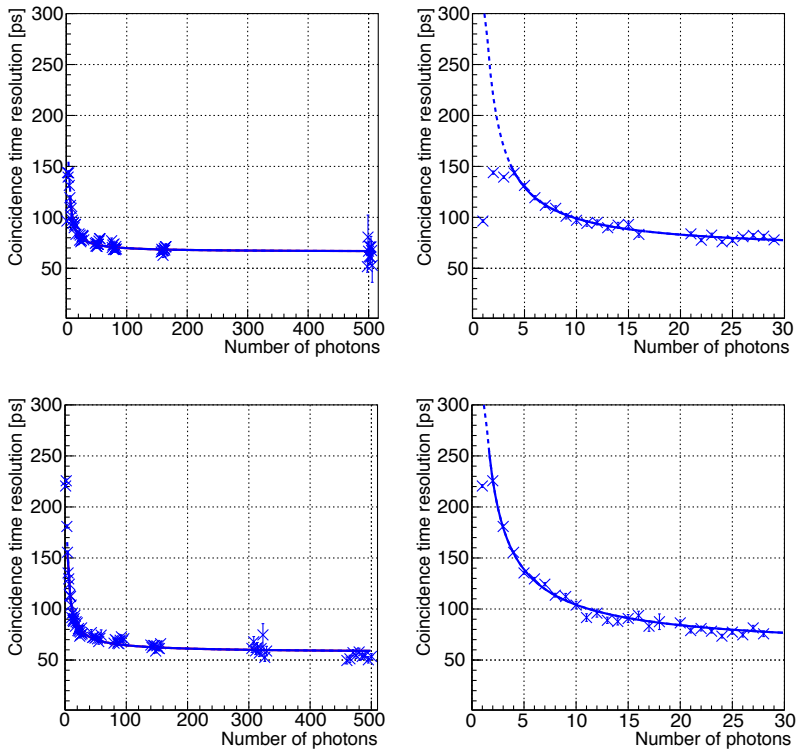

Figure 4. The DPC time resolution measurements in terms of FWHM, for the DPC3200 die at 10°C (top) and the DPC6400 die at 0°C (bottom). On the abscissa the number of photons refers to the exact number of photons detected at each die/pixel. The data was selected for events where the same number of photons was recorded on both dies/pixels. Each data point was determined from a Gaussian fit of the timing histogram. On the left-hand side all measured data points are shown, whereas on the right-hand side a zoom of the data can be seen. The blue line represents a fit based on equation (3.1). The dashed lines are extrapolations to single-photon level as described in the text. In both detectors the 20% of SPADs with the highest dark-count rates were deactivated.

with p_0 representing the TR relative to the system TR, p_2, and p_1 representing the TR as a function of the number of photons. The system TR is determined as the saturation value of $TR(n)$ at high photon numbers. In this regime, the TR is mainly influenced by time pick-off jitter, TDC jitter, and clock jitter [17].

One can see that the fits in figure 4 describe the measured data well over a wide range of photon numbers, but deviate from this data at low photon numbers. This effect has already been observed by Frach et al. [11]. In figure 5, the time-delay histograms of one exemplary data-set measured with two dies of the DPC3200 sensors in coincidence are shown, starting from single-photon level (i.e., two single photons in coincidence) up to 3-photon level including the corresponding Gaussian fits. A detailed investigation of the unexpected behaviour at low photon intensities has been performed by Brunner [16], using simulation and experiments. The improvement of the time resolution at very low photon numbers was found to be an artefact related to cross-talk. An explanation of this cross-talk phenomenon could be connected to optical photon emission during discharge of the SPADs. The emitted photons might be internally reflected at the surface of the quartz-protection

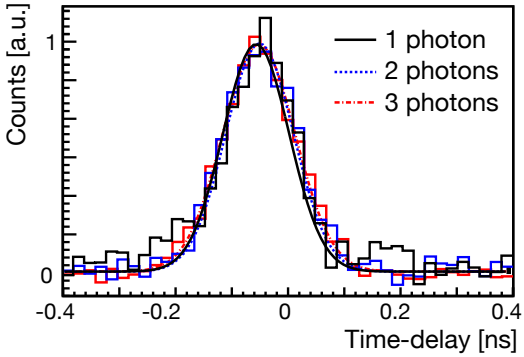

Figure 5. Time-delay histograms measured for 2 dies of the DPC3200 sensor in coincidence (20% of the most active SPADs deactivated, 10°C). The time delay histograms are plotted from single-photon level (two single photons in coincidence) up to 3-photon level and the corresponding Gaussian fits (data taken from one exemplary data-set).

Table 1. Extrapolated single photon time resolution (SPTR), in terms of FWHM and system time resolution, of the Philips DPC for various measurement conditions. It is to be noted that the SPTR includes the system time resolution.

DPC	Active area	Temp. [°C]	Inactive cells [%]	SPTR FWHM [ps]	System TR FWHM [ps]
3200	die	0	0	187 ± 5.9	47 ± 1.9
3200	die	0	20	168 ± 3.0	42 ± 0.8
3200	die	0	50	153 ± 2.3	45 ± 0.6
3200	pixel	10	20	101 ± 2.8	16 ± 2.4
3200	pixel	20	20	113 ± 3.5	14 ± 3.1
6400	die	0	20	247 ± 3.0	40 ± 0.4

glass that is covering the sensor and may trigger correlated events in neighbouring SPADs. This hypothesis is supported by experiments using a picosecond laser which revealed that the observed artefact decreases when the distance between the active dies/pixels was increased.

As the single photon time resolution (SPTR) could not be determined directly, it was found by fitting the data in the range from 2 - 4 photons up to the maximum measured value (full lines in figure 4), followed by extrapolation of the obtained function to the single-photon level (dashed lines in figure 4). The results for the SPTR of a single sensor die are summarised in table 1.

Comparing the values in the table it can be seen that the SPTR improves with decreasing number of active cells. This effect can be explained mainly by a reduced influence of the trigger network skew when the number of active cells is decreased [18]. The best SPTR for a complete die was found with 50% of the SPADs deactivated, resulting in 153 ps FWHM ± 2.3 ps FWHM. For a more realistic scenario of 20 % deactivated cells a SPTR of 168 ps FWHM ± 3.0 ps FWHM was observed. This configuration was kept when the SPTR of a pixel was determined, resulting in an SPTR of 101 ps FWHM ± 2.8 ps FWHM at 10°C.

For the DPC3200 sensor, system time resolutions between 42 ps FWHM and 47 ps FWHM were found when complete dies were investigated. For single pixels the system TR improves to values between 14 ps FWHM to 16 ps FWHM. These values agree with the results reported by Frach [18]

2016 JINST 11 P11004

and are related to reduced trigger network skews and, thus, an improved time jitter if only one pixel is activated.

3.2 SPAD time resolution

In a further step the time resolution of individual SPADs was determined. The measurements were performed at a constant temperature of 10°C. Two cases were investigated for the DPC3200 sensor:

- variable laser power and only one SPAD active on each of the two illuminated dies,
- variable number of active SPADs on two dies at constant laser power.

The laser intensity was calibrated by activating 90 % of the SPADs on one die and counting the mean number of detected photons with different combinations of neutral density filters. This was done from levels around one photon per die per pulse up to about several hundred photons, i.e. within a region where a linear response of the DPC can be expected. Fitting the measured numbers of photons using a linear function, a calibration curve for the laser intensity was generated. This calibration curve was then extrapolated to very high and low laser intensities and used for other combinations of neutral density filters. The average laser intensity impinging on a SPAD was be calculated by dividing the number of counted photons during calibration by the number active SPADs on a die. It should be noted that it is not the true number of impinging photons but the number of photons actually triggering an avalanche that is determined in this way.

In the following paragraphs the major steps of avalanche processes in SPADs are described qualitatively before necessary statistical considerations for adequate interpretation of the observed SPAD time resolution is discussed.

Avalanche growth processes in SPADs Several scenarios for avalanche generation in SPADs need to be distinguished in order to understand their observed time resolution. The discussed processes are depicted in figure 6. This figure schematically shows the the cross-section of a SPAD with a typical doping structure for blue-light sensitive SPADs produced in CMOS technology such as those used in the Philips DPC. Between the anode (p+) and the (n+)-doped layer of the SPAD, a depleted region of typically a few µm is generated when reverse bias is applied. Above the breakdown voltage, the field in the depleted region is sufficiently high that a self-sustaining avalanche can be triggered by impact-ionization after injection of a single charge-carrier in this region.

Two major contributions to the SPAD time resolution need be distinguished: the statistical variation of the avalanche growth and the influence of the location of charge-carrier generation. The statistical variation of the avalanche build-up is influenced by the avalanche propagation mechanisms depicted in figure 6, i.e., build-up of the avalanche by exponential carrier-multiplication in the longitudinal direction (I), followed by lateral diffusion of the charge-carries at the avalanche front (II), and photon-assisted propagation (III). The statistical nature of the avalanche growth by charge-carrier diffusion represents a major factor limiting the time resolution of a SPAD in general. Furthermore, the average speed of the avalanche build-up, and thus the time jitter, can be influenced by the field strength distribution in the depletion layer [19–21].

Besides the statistical variation of avalanche growth, it has been shown that the location of charge-carrier injection influences the time resolution of the SPAD [22–24]. The following

2016 JINST 11 P11004

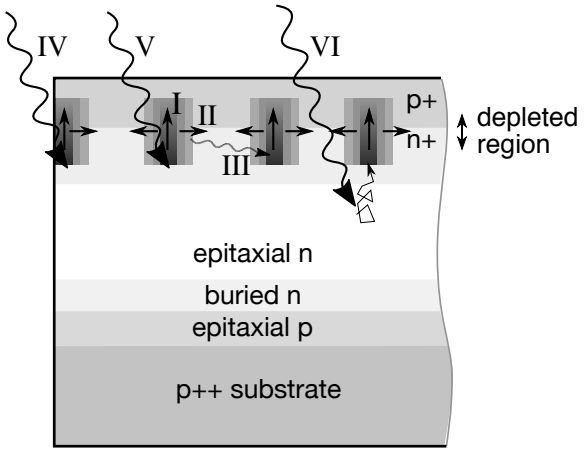

Figure 6. Schematic of possible avalanche growth processes occurring in SPADs: longitudinal (I), lateral (II) and photon assisted avalanche growth (III). Localisation of the charge-carrier injection at the edge of a SPAD (IV), directly in the depletion region (V) and avalanche breakdown after electron diffusion toward the depleted region (VI) are also indicated.

simplified scenarios can be distinguished: case (IV) of figure 6 shows avalanche spread at the edge of the SPAD where the direction of the avalanche build-up is limited by spatial (field) constraints resulting in a slower build-up. Case (V) shows the photoelectric interaction of the impinging optical photon in the depletion region. The released photoelectron can trigger the build-up immediately. In case (VI) the photon is interacting in the epitaxial n-doped layer beneath the depletion region. Here the charge carrier needs to diffuse towards the depletion region before an avalanche can be initiated. According to literature this effect is giving rise to a diffusion tail and adds in additional time jitter to the avalanche build-up [21, 24]. As the penetration depth of blue light is small, the influence of charge diffusion is likely to have a relatively small impact on the observed time resolution presented in this work.

Statistics of triggering photons In order to understand the presented results of the SPAD TR also the statistical nature of the number of photons triggering an avalanche needs to be discussed. The following derivation addresses the variation of the number of photons simultaneously triggering an avalanche in each SPAD when considering a coincidence-setup of two SPADs. The result of this discussion is plotted as dashed grey line in figure 7 and explains why the values of the time resolution at very low light intensities can be interpreted as the SPTR of the SPAD. More precisely, this curve represents the probability that an avalanche is triggered by exactly 1 photon in each SPAD and can be derived starting from a Poisson distribution for the laser intensity per pulse

$$P_{\text{laser}}(\lambda, n) = \frac{\lambda^n e^{-\lambda}}{n!}, \tag{3.2}$$

with n the number of photons hitting a given SPAD and λ the average laser intensity. For the case that exactly one photon is triggering an avalanche in the SPAD the probability distribution is evaluated for $n = 1$.

2016 JINST 11 P11004

Additionally, the experimental condition that events are only recorded when ≥ 1 photons are impinging a SPAD is met can be expressed as follows,

$$P_{\text{trigger}}(\lambda, n \geq 1) = 1 - P(\lambda, n = 0) = 1 - e^{-\lambda}. \tag{3.3}$$

Moreover, at average laser intensities smaller than 1 photon per pulse, multiple pulses are needed to trigger an avalanche eventually. The SPAD thus registers an event in a fraction $1/P_{\text{trigger}}(\lambda, n \geq 1)$ of the pulses, giving a probability for a discharge to be triggered by exactly 1 photon

$$P_{\text{las.trig.}}(\lambda, n = 1) = \frac{\lambda e^{-\lambda}}{1 - e^{-\lambda}}. \tag{3.4}$$

Eventually, the condition of detecting only coincident events is met by squaring the obtained probability,

$$P(\lambda, n = 1)^{\text{coinc.}}_{\text{las.trig.}} = \left(\frac{\lambda e^{-\lambda}}{1 - e^{-\lambda}}\right)^2. \tag{3.5}$$

This function represents the probability that a registered coincident event is triggered by exactly a single photon in each SPAD. Following this function in figure 7, the probability that exactly one photon is triggering an avalanche in each of the two SPADs is 0.95 in the region a, decreasing to about 0.6 in region b and approaching zero when moving on to regions c and d. Region b is a special case: in this region of average laser intensity of a single triggering photon per SPAD per pulse it is possible that coincidences are not triggered by a single photon on each SPAD but, e.g., by two photons in one SPAD and by a single photon in the other SPAD. As the build-up is likely to be faster when more than one photon is initiating an avalanche the variation of the number of triggering photons give rise to the increased time jitter observed.

SPAD-TR for variable laser intensities In this measurement only a single SPAD on each of two adjacent dies was activated and the laser intensity was varied. The results obtained are plotted in figure 7 on the left, while two example histograms of the results are shown on the right side of the same figure. They can be interpreted and understood as follows (the letters refer to the letters in the figure):

(a) *SPTR of the SPAD* — This value represents the time resolution of a single SPAD when only a single photon is triggering the avalanche. The value for the SPAD SPTR obtained is 48.2 ps FWHM ± 0.4 ps FWHM. Several effects are influencing this value, including the electronics jitter (i.e., time pick-off variations due to noise, TDC jitter and clock distribution jitter), the statistical nature of longitudinal and transversal build-up of the avalanche in the high-field region of the p-n junction [19, 20], and the variation of the avalanche build-up time with the location of the triggering photon, i.e., time spread due to electron diffusion towards the depleted region and especially slower avalanche build-up due to border-effects (scenarios I-VI of figure 6) [23, 24].

A schematic drawing for the corresponding current signal and the time pick-off in this regime is shown in figure 8a. Repeating the measurement would result in a time-delay histogram as drawn on the right-hand side of the figure, providing the TR of the SPAD at single-photon level.

2016 JINST 11 P11004

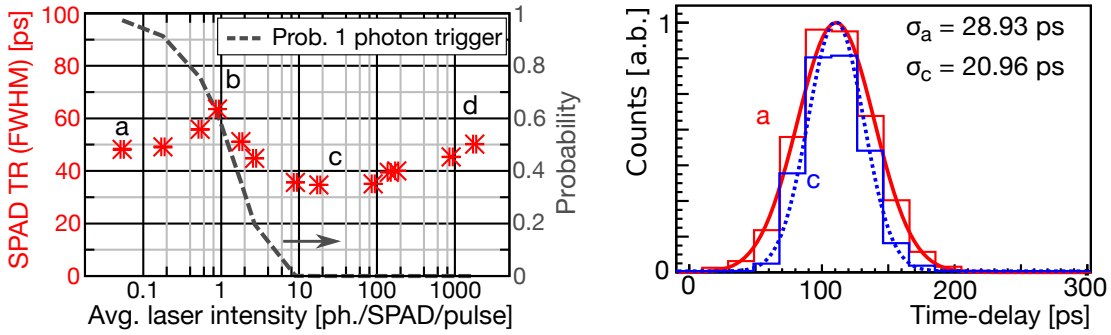

Figure 7. The time resolution (TR) of single SPADs was determined for various numbers of simultaneously impinging photons. The left plot shows the SPAD time resolution dependent on the number of photons registered by the SPAD per pulse. As explained in the text, different regimes can be distinguished: (a) TR at single-photon trigger, (b) TR influenced by statistical noise, (c) TR at a high number of triggering photons, and (d) TR deterioration due to the influence of space-charge or dead-space effects. Additionally, the probability that a coincidence event was triggered by exactly one photon on each of the two SPADs is indicated by the grey dashed line. On the right side two example histograms for regimes (a) and (c) are drawn. Additionally, the standard deviations (σ) of the Gaussian fits are given. The SPAD SPTR in terms of FWHM is obtained by multiplying the standard deviation by $2.35/\sqrt{2}$.

(b) *Degradation by statistical fluctuation of triggering photons* — With increasing laser intensity, an increase of the time resolution is initially observed. This may be correlated with the statistical fluctuation of the number of photons triggering the SPAD per pulse. More precisely, the variance of the laser intensity is increasing from very low laser intensities (where the variance approaches zero) up to about one photon per SPAD per pulse, leading to a worsening of the SPAD time resolution. The details were discussed earlier in this section under 'Statistics of triggering photons'. This behaviour can be understood by looking at figure 8, case (b): in this regime it is likely that the event was triggered not by one but also by two or more photons. Although fluctuations due to border-effects of the avalanche are statistically reduced when multiple photons are triggering the SPAD simultaneously (dashed signal curves) the large relative variance in the number of triggering photons (varying between one and a few per SPAD) may result in a broadening of the convoluted time-delay histogram.

As mentioned before, the probability distribution for pure single-photon coincidences is drawn at the left plot of figure 7 (grey dashed line). From this curve it can be seen that the probability of a coincidence not being triggered by a single photon on both SPADs is about 0.4. From pulse to pulse the number of triggering photons varies around the average laser intensity of 1 photon per pulse per SPAD. On average, the built-up appears to be faster when more photoelectrons trigger an avalanche in the SPAD simultaneously due to the increased probability that one of those photoelectrons was created inside the depletion region or at a central location of the SPAD (compare with signal response drawn as dashed lines in figure 8b). In this case the leading edge of the current signal, and consequently the recorded timestamp, are observed earlier. As a result of the variation of the number of impinging photons, the time resolution appears to be worse in this regime.

(c) *Single SPAD time resolution at high intensities* — If the laser intensity is increased further, more and more photons are simultaneously triggering the SPAD, resulting in an increasing probabil-

2016 JINST 11 P11004

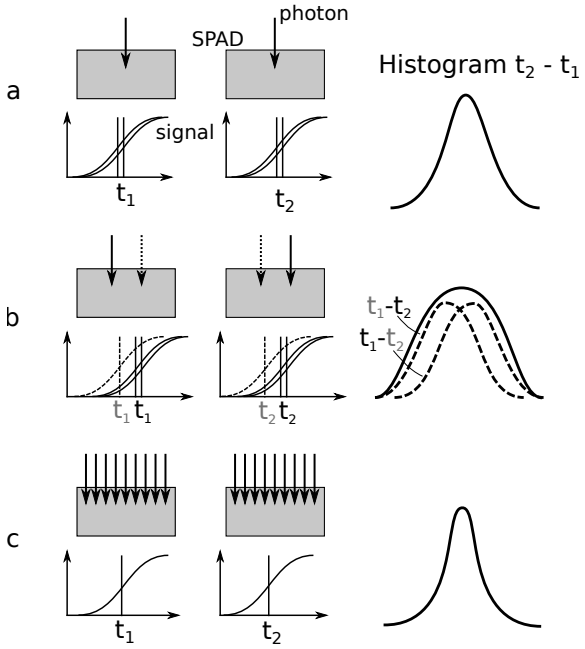

Figure 8. Schematic drawing explaining the variation of the single-SPAD time resolution with increasing average laser intensity (see text for details). Different time resolutions are found in the regimes of (a) very low laser intensity, (b) average laser intensity of about one photon per SPAD per pulse, and (c) average laser intensity of about 10 to 100 photons per SPAD per pulse. At the bottom-left side of each drawing the resulting variations in the SPAD current signal and the corresponding variations in the time pick-off (t_1 and t_2) are depicted schematically, resulting in the time-delay histograms for repeated measurements of $t_2 - t_1$ on the right-hand side. The width of the histograms on the right-side is caused by avalanche statistics of the SPADs and not by the statistical distribution of the photons within the laser pulse. For scenario (b) the dashed arrows indicate a second photon triggering an avalanche. In this case earlier time-pickoff is observed earlier than compared to only one photon hitting the SPAD (explanation in text). The variation in the number of triggering photons and thus the time-pick-off causes the observed increase of the SPAD TR in region (b) of figure 7 on the left side.

ity for fast breakdown, especially initiated by photoelectrons created inside the depletion region and improving the observed SPAD time resolution (c). The time resolution is finally reaching a minimum in the range of 10 to 100 photons per SPAD per pulse. This minimum represents the single SPAD time resolution including electronics jitter and the intrinsic statistical variations of the avalanche build-up inside the depletion region (especially case I of figure 6) as border and diffusion effects are masked by the high number of initial photoelectrons [24, 25].

(d) *Saturation effects* — When increasing the laser intensity even further, the time resolution worsens again. This effect has been reported already by Fishburne et al. [24]. It might be related to space-charge or dead-space effects during avalanche build-up, as described by Spinelli et al. and Yamamoto et al. [19, 23] but is not understood so far.

Eventually, it should be noted that the influence of the laser time-jitter can be neglected. Moreover, the measured CRT is caused by avalanche build-up statistics of the SPADs and inaccuracies of the DPC-electronics and not by the statistical distribution of the photons within the laser pulse.

2016 JINST 11 P11004

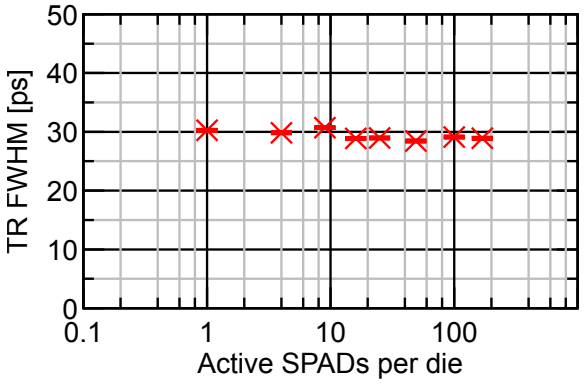

Figure 9. Time resolution (TR) as a function of the number of SPADs per die at a laser intensity of about 30 registered photons per SPAD per pulse.

Overall, the distribution found is in agreement with the observations made for measurements of analogue SPADs as published by E. Popova [25]. Moreover, the measurement is qualitatively in good agreement with the experimental investigations on multi-photon triggering of CMOS-SPADs by M. Fishburne et al. [24]. As Fishburne et al. were using the laser trigger signal for detecting coincidences they did not observe increase of the TR at mean laser intensities of about one photon per pulse (figure 7, case (b)).

It is worth mentioning that, although the CMOS process used for manufacturing the DPC is challenging, the time resolution obtained for a single SPAD is in the same range as for the SPADs of analog SiPMs with comparable size [26].

Variable number of SPADs In a second measurement the laser intensity was kept constant at about 30 registered photons per SPAD and the number of activated SPADs on two adjacent dies was varied. The results can be seen in figure 9. The time resolution determined with one SPAD per die activated was 30.28 ps FWHM. This value includes contributions of the readout electronics (TDCs, clock distribution jitter), but excludes the trigger network skew [18].

The best value of 28.4 ps FWHM was obtained when an array of 7×7 SPADs per die was activated. However, the overall time resolution remains more or less constant up to the maximum number of activated cells. This can be explained by the fact that at 30 triggering photons per SPAD per pulse the SPADs with the shortest lines to the TDC are always triggering the TDC, no matter how many SPADs are active. Therefore, in this configuration, the mean values of the obtained TOF spectra can change with a changing number of active SPADs but the standard deviation of the timing distribution remains essentially constant.

4 Conclusion

In this study the timing characteristics of the Philips DPC are investigated using a femtosecond laser. It is shown that the time resolution of the device varies with temperature and number of activated cells. The single photon time resolution of a single die of the DPC3200 array was measured to be 153 ps FWHM under the best configuration, while the best value obtained for a single pixel was 101 ps FWHM. The contribution of the electronics (TDC and clock distribution jitter) of the

2016 JINST 11 P11004

DPC3200 array to the overall SPTR was found to be between 42 ps FWHM and 47 ps FWHM, which for a single pixel improves to values between 14 ps FWHM and 16 ps FWHM. The SPTR of a die of the DPC6400 array was found to be 247 ps FWHM, comprising an electronics contribution of 40 ps FWHM.

Furthermore, the time resolution of a single SPAD of the DPC3200 array was found to be 48 ps FWHM if a single photon is triggering the avalanche. Additionally, it was shown that, at laser intensities of about 30 photons per pulse per SPAD, the time resolution maintains a constant value of about 30 ps FWHM for 1 up to 150 simultaneously activated SPADs per pixel. This shows that the time resolution is independent of the number of active SPADs under saturating conditions, as the influence of the trigger network skew is vanishing.

Acknowledgments

We would like to kindly thank Herbert Orth for his long lasting and extensive support and for the provision of the Philips DPCs and Esteban Venialgo from TU Delft for the nice and revealing discussions. Finally, we also would like to thank Femtolasers GmbH, Vienna for their support of the measurements with provisioning of the laser infrastructure.

This work was partly funded by the European Research Council under European Union's Seventh Framework Programme (FP7/2007- 2013)/ERC Grant agreement (291242) and supported by European Union's Horizon2020 Framework Programme Marie Skłodowska-Curie action (659317).

References

[1] S. Seifert et al., *A Comprehensive Model to Predict the Timing Resolution of SiPM-Based Scintillation Detectors: Theory and Experimental Validation*, *IEEE Trans. Nucl. Sci.* **59** (2012) 190.

[2] D.R. Schaart et al.,*LaBr(3):Ce and SiPMs for time-of-flight PET: achieving 100 ps coincidence resolving time.*, *Phys. Med. Biol.* **55** (2010) N179.

[3] M.V. Nemallapudi et al., *Sub-100 ps coincidence time resolution for positron emission tomography with LSO:Ce codoped with Ca*, *Phys. Med. Biol.* **60** (2015) 4635.

[4] J.W. Cates and C.S. Levin, *Advances in coincidence time resolution for PET*, *Phys. Med. Biol.* **61** (2016) 2255.

[5] S.E. Brunner et al., *Comparative Study on the Time Resolution of Co-Doped LSO:Ce, LYSO:Ce and LFS*, submitted to *IEEE NSS-MIC*, Strassbourg (2016).

[6] Philips Vereos Digital PET-CT, *Philips U.S.A. webpage*, http://www.usa.philips.com/healthcare/product/HC882446/vereos-digital-pet-ct (April 2016).

[7] General Electric Signa PET/MR, *General Electric webpage*, http://www3.gehealthcare.com/en/products/categories/magnetic_resonance_imaging/signa_pet-mr (April 2016).

[8] H.T. van Dam, G. Borghi, S. Seifert and D.R. Schaart, *Sub-200 ps CRT in monolithic scintillator PET detectors using digital SiPM arrays and maximum likelihood interaction time estimation*, *Phys. Med. Biol.* **58** (2013) 3243.

[9] G. Borghi, V. Tabacchini and D.R. Schaart, *Towards monolithic scintillator based TOF-PET systems: practical methods for detector calibration and operation*, submitted to *Phys. Med. Biol.*

2016 JINST 11 P11004

[10] G. Borghi, B.J. Peet, V. Tabacchini and D.R. Schaart, *A 32 mm × 32 mm × 22 mm monolithic LYSO:Ce detector with dual-sided digital photon counter readout for ultrahigh-performance TOF-PET and TOF-PET/MRI*, submitted to *Phys. Med. Biol.*

[11] T. Frach, G. Prescher, C. Degenhardt, R. de Gruyter, A. Schmitz and R. Ballizany, *The digital silicon photomultiplier: Principle of operation and intrinsic detector performance*, *IEEE Nucl. Sci. Symp. Conf. Rec. — NSS/MIC* (2009), pp. 1959–1965.

[12] R. Schulze, *Tile-TEK Manual v1.00*, Philips Digital Photon Counting (2015).

[13] V. Tabacchini, V. Westerwoudt, G. Borghi, S. Seifert and D.R. Schaart, *Probabilities of triggering and validation in a digital silicon photomultiplier*, 2014 *JINST* **9** P06016.

[14] S. Seifert, H.T. van Dam and D.R. Schaart, *The lower bound on the timing resolution of scintillation detectors*, *Phys. Med. Biol.* **57** (2012) 1797.

[15] S. Mandai, E. Venialgo and E. Charbon, *Timing optimization utilizing order statistics and multichannel digital silicon photomultipliers*, *Opt. Lett.* **39** (2014) 552.

[16] S.E. Brunner, *Fast single photon detection for scintillation and Cherenkov applications using Silicon Photomultipliers*, PhD thesis, Vienna University of Technology, Vienna, Austria (2014).

[17] Y. Haemisch, T. Frach, C. Degenhardt and A. Thon, *Fully Digital Arrays of Silicon Photomultipliers (dSiPM): a Scalable Alternative to Vacuum Photomultiplier Tubes (PMT)*, *Phys. Procedia* **37** (2012) 1546.

[18] T. Frach, *Optimization of the digital Silicon Photomultiplier for Cherenkov light detection*, 2012 *JINST* **7** C01112.

[19] A. Spinelli and A. Lacaita, *Physics and numerical simulation of single photon avalanche diodes*, *IEEE Trans. Electron Devices* **44** (1997) 1931.

[20] A. Lacaita and M. Mastrapasqua, *Strong dependence of time resolution on detector diameter in single photon avalanche diodes*, *Electron. Lett.* **26** (1990) 2053.

[21] M. Assanelli, A. Ingargiola, I. Rech, A. Gulinatti and M. Ghioni, *Photon-timing jitter dependence on injection position in single-photon avalanche diodes*, *IEEE J. Quantum Electron.* **47** (2011) 151.

[22] G. Ripamonti and S. Cova, *Carrier diffusion effects in the time-response of a fast photodiode*, *Solid State Electron.* **28** (1985) 925.

[23] K. Yamamoto et al., *Development of Multi-Pixel Photon Counter (MPPC)*, *IEEE Nucl. Sci. Symp. Conf. Rec.* **2** (2007) 1511.

[24] M.W. Fishburn and E. Charbon, *Distortions from multi-photon triggering in a single CMOS SPAD*, *Proc. SPIE* **8375** (2012) 83750O.

[25] E. Popova, *Timing with SPADs: Critical Parameters*, talk at meeting of *EU-COST project Fast Scintillator Timing (FAST)*, April 2015.

[26] F. Acerbi et al., *Characterization of Single-Photon Time Resolution: From Single SPAD to Silicon Photomultiplier*, *IEEE Trans. Nucl. Sci.* **61** (2014) 2678.

2016 JINST 11 P11004